

Energy and Exergy Analysis of a Multi-PCM Solar Storage System

Wisam H. Mousa^{1,*}, Fawziea M. Hussein¹, Johain J. Faraj¹

¹ Middle Technical University, Technical Engineering College, Baghdad, Iraq

ARTICLE INFO

Article history:

Received 7 July 2020

Received in revised form 12 August 2020

Accepted 12 August 2020

Available online 19 November 2020

Keywords:

Phase change material (PCM); Latent heat storage unit (LHSU); Solar collector; exergy analysis

ABSTRACT

Latent heat storage using phase change materials (PCMs) is one of the most effective methods to store solar energy, and it can significantly reduce area for solar collectors. PCMs are isothermal in nature, and thus offer higher density energy storage and the ability to operate in a variable range of temperature conditions. In this paper, experimental study has been conducted to evaluate the effectiveness of the solar thermal storage system based on the energy and exergy analysis. Barium Hydroxide Octahydrate (BHO) and Sodium Acetate Trihydrate (SAT) were used as PCMs inside multi-capsule system arranged in series based on their melting temperatures. These two salts never being used together in a multi capsule solar storage system before. The capsules were charged by three water flow rates of 0.5 LPM, 1 LPM and 1.5 LPM that comes from a parabolic trough collector. The experimental results showed that the maximum energy and exergy storage of 139.38 kJ and 17.15 kJ, respectively were obtained from 1 LPM. In other hand, the maximum system energy and exergy efficiencies of 64.82 % and 14.99 %, respectively were obtained from the use of 1.5 LPM.

1. Introduction

Energy crisis is one of the biggest problems facing the world for decades caused by the industrialization, rapid population growth, rising of living standards. Traditional energy resources such as petroleum, coal and natural gas takes about 80 % of the commercial energy global production [1]. However, the researchers have been motivated to find alternative clean energy resources to overcome the conventional limited energy that harmed the human health with serious environmental effects due to high CO₂ emissions [2]. The solar energy has been emerged as suitable solutions to many environmental problems. The renewable energy sources are intermittent by nature so that they require a storage system. One of the most considerable and important storage

* Corresponding author.

E-mail address: wisamhamdan599@gmail.com

<https://doi.org/10.37934/arfmts.78.1.6078>

systems, are the Thermal Energy Storage (TES) systems. These systems come with two types, sensible heat thermal energy storage (SHTES) and latent heat thermal energy storage (LHTES) [3]. To achieve a high-density storage system with higher efficiency, a modern method has been proposed to use the Phase Change Material (PCM) in these systems. PCMs have been widely used in the latent heat storage systems for solar engineering, heat pumps and spacecraft thermal control applications [4]. Salt hydrates are the most important group of PCM that have been extensively investigated and used for thermal energy storage applications. The most attractive properties of salt hydrates are: (1) high latent heat of fusion (2) relatively high thermal conductivity as compared to other types of LHTES and (3) small volume change during the phase change process. In addition, the salt hydrates are cheap and abundantly available which makes them commercially attractive for thermal energy storage applications. Along with above, the salt hydrates are compatible with plastic containers and show lower toxicity. For outdoor conditions in solar applications, the transition temperature should be in the range of 50 °C to 80 °C in most cases. Among the PCMs, Sodium Acetate Trihydrate (SAT) and Barium Hydroxide Octahydrate (BHO) are the materials that can meet these required properties. The melting points of them are between 58 and 78 °C, which are just in the temperature range of the solar energy systems [5].

Englmair *et al.*, [6] built a laboratory solar heating system with heat-pipe tubular collectors in aperture and a heat-storage unit consisting of a 735 L water tank and four PCM units each containing 200 kg of sodium acetate trihydrate composite. Operation was demonstrated with the space heating and hot water demand patterns of a standard-size Passive House. During the charging of PCM units, the flow temperature was kept between 70 °C and 95 °C to allow continuous heat transfer rates of up to 16 kW. Peaks of up to 36 kW occurred when PCM units were added to the charging circuit. During heat transfer from PCM units to the water tank, flow temperatures were close to the SAT composite temperature and thermal power of up to 6 kW was measured. Sodium acetate trihydrate was studied by Zhiwei *et al.*, [7] as a seasonal solar thermal energy storage material. For a single tube storage system with 10.51–10.65 kg PCM, the HTF outlet temperature could reach 30.4–37.5 °C when the ambient temperature was in the range of 0–15 °C and the mass flow rate of HTF was 0.001 kg/s. This indicates the quality of discharged heat was enough to do space heating. The corresponding output thermal power was in the range of 94.0–127.7 W. Five nucleating agents have been added to BHO by Wang *et al.*, [8] to suppress the supercooling phenomena, including sodium borate, copper powder, calcium fluoride, calcium chloride and Calgon. The experimental results indicated that the addition of 1% copper powder, 1% calcium fluoride, and 1% Calgon by weight can reduce the supercooling degree to 2.7 °C, 1.8 °C and 2.3 °C respectively. Thomson, A. and Claudio, Gianfranco [9] investigate the feasibility of utilizing phase change materials (PCM) for thermal energy storage (TES) within district heating applications (DHN). The increased storage capacity associated with PCM can reduce cycling of plant which in turn can increase lifespan and improve the overall system performance. The results suggest that PCM such as Sodium Acetate Trihydrate can be economically and environmentally feasible when utilized for TES in DHN. Air pollution and CO₂ emissions can be reduced through the increase in heat pump contribution. A CFD mathematical simulation was introduced by Kadhim *et al.*, [10] to investigate the temperature distribution over the time for water flowing inside the pipes of solar collector and the PCM placed on the back layer of the collector as a storage media. The simulation results give that the maximum outlet water temperature is (58 °C) at (4:00 PM), while the maximum temperature of PCM is (54 °C) at (5:00 PM). The water temperature is higher than that PCM temperature at the day hours (PCM Charge). Also, the PCM was capable to charge the water with the required energy during the night. Bayomy *et al.*, [11] conducted numerically a three-dimensional model of a water thermal storage tank to provide domestic hot water demand. Phase change material was used in the tank as a thermal medium and was connected

to a photovoltaic thermal collector. The results indicated that the increase in the hot water supply increased the storage efficiency from 35 % to 39 % during the charging periods. For a given hot water flow rate, increasing the number of families from one to four, increased the system efficiency from 35 % to 82 %, respectively. An exergy analysis was conducted by Nagappan *et al.*, [12] on the evacuated tube parabolic trough collector connected to a cascaded latent heat storage system. The overall exergy efficiency improvement of the collector was 5.9 %. The results showed that the exergy stored for 5 and 10 LPM water flow rates were 24.609 kW and 40.48 kW, respectively. Li *et al.*, [13] proposed a new solar collector and storage system using erythritol as a PCM. A mass fraction of 3 % of the expanded graphite was added to the PCM. A numerical model was established and experimentally validated based on the enthalpy-porosity models. The experimental results showed that the daily average storage efficiency of the system reached to 39.98 %. The simulation results indicated that the storage efficiency reached a value of 34.3 %.

Barium hydroxide octahydrate and Sodium acetate trihydrate are promising low temperature phase change materials, which have a high latent heat capacity and a relatively large thermal conductivity. Therefore, as previous works did not investigate these two salts together in a solar storage unit, this work aim to study the thermal performance of multi capsules solar energy storage system that works with BHO and SAT together. The two salts were connected in series based on the melting temperatures to investigate the storage unit based on the energy and exergy analysis.

2. Materials and Methods

The parabolic trough was made from 5.7 mm metal strips that were cut by CNC machine. A chromium steel sheet of 0.6 mm with dimensions of (171.5 x 100 cm) was chosen as a reflective surface for the parabolic trough collector. It was screwed to the parabolic frame. The evacuated tube is made of a glass coated with an absorber material from the inside. An aluminum sheet was inserted inside the evacuated tube to ensure two passes water flow as it had just one open end. The parabolic dimensions data are listed in Table 1, it is the smallest standard one found in the market that could generate a temperature high enough to melt the salts. The PCM capsule is consisted of four welded enclosures of (40 x 40 x 150 mm) made of 1 mm thickness aluminium as shown in Figure 1. Two of these enclosures worked as water passages with two pipe connections. These pipe connections are welded to the enclosure from lower front and upper behind for water inlet and outlet respectively. The other two enclosures are worked as PCM containers that opened from above. These containers are frontal covered with a piece of glass for clear view of the melting and solidification processes of the PCM. These containers are welded side by side while each of the water passages enclosures are welded besides each of the containers. Two aluminum rods of 10 mm diameter and 150 mm length can be inserted inside each container. These rods held three thermocouples vertically distributed at 37.5 mm for PCM temperature measurements. The capsule is covered with cork for thermal insulation as it connected with the piping system.

Table 1
Parabolic Trough Collector Data

Parameters	Dimension
Collector Aperture Length	171.5 cm
Collector Aperture Width	84 cm
Focal Distance	18.04 cm
Rim Angle	99 °
Aperture Area	14406 cm ²
Evacuated Tube Length	175 cm
Glass Diameter	5.8 cm
Absorber Diameter	4.5 cm
Receiver Surface Area	2424.45 cm ²
Concentration Ratio	5.942

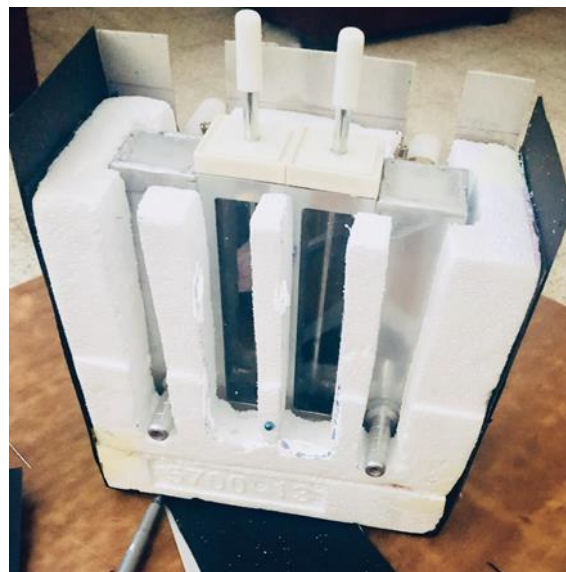


Fig. 1. The Capsulated Assembly

The schematic diagram of the test rig system is shown in Figure 2. The components assembly of the test rig with the data logger system as shown in Figure 3. The parabolic trough collector is connected to right side of the capsule due to a water pump that is draw clean water from an insulated water tank. The left side of the capsule is connected to another water pump that takes the water from the main line of the house. Two kind of temperature sensors were used in this project. The first one is the DS18B20 waterproof temperature sensor. This sensor has a temperature range of -55 °C to 125 °C with 0.5 °C accuracy. Four DS18B20 sensors were used to measure the temperature of water for the inlet and outlet streams of both hot and cold sides of the capsule. Thermocouples type K also used to measure the temperature distribution of the PCM in the both containers during the melting and solidification processes. The k-type thermocouples having a range of 0 – 1024 °C. The Water Flow Sensor YFS201 works on the principle of the Hall effect. The YFS201, measures water flow rates up to 30 L/min under maximum water pressure of 2 MPa. These sensors were connected to a data logging system of an Arduino MEGA. The thermal storage system parts were connected together with the measuring devices. After checking the system for leakage, the hot and cold sides capsules were filled with 200 g of each PCM.

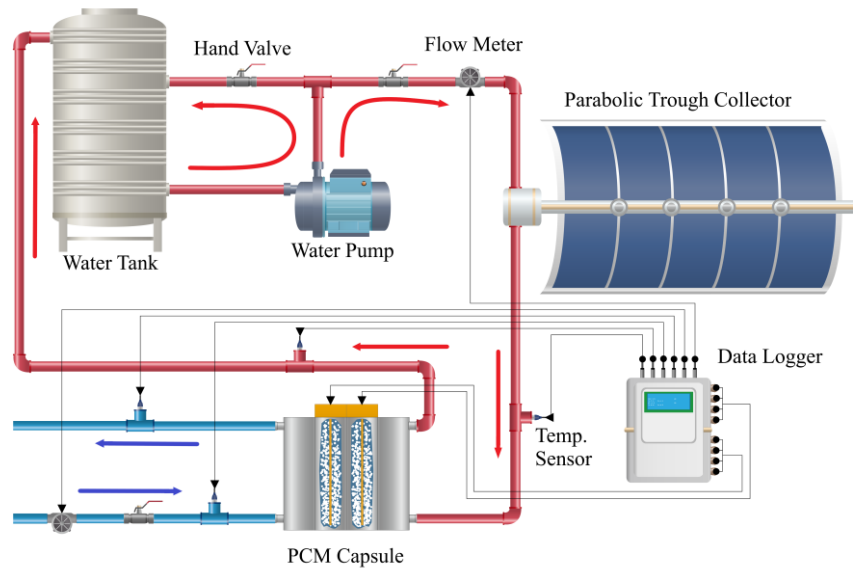


Fig. 2. The Schematic Diagram of the System



Fig. 3. The Whole System with Insulated Tank

3. Energy and Exergy Analysis

Some models are designed to measure the energy efficiency as first law of the thermodynamics. The first law of thermodynamic focus on the quantity of energy, while the second law explains the exergy analysis taking into accounts the quality, irreversibility and usefulness of the energy. The second law models deal with the issues which influence optimum design and operation. First law models do not consider the surroundings effects like pressure and temperature, which energy is stored or recovered during charging or discharging processes. Therefore, the first law shows how energy is utilized whereas the second law model indicates how the accessibility of energy is used. Meanwhile the exergy is produced as the maximum quantity of work that the system comes to equilibrium with surrounding. On the other hand, the system cannot be retained back to primary performance during the charging and recharging operation and irreversibility concept is shown numerically by exergy. Energy and exergy analysis for multi PCMs storage system is came out as an

important solution for utilization of solar thermal storage systems [14]. The energy produced by the hot water or taken by the cold water can be calculated by [15]

$$Q_w = \dot{V}_w \rho_w C_{pw} (T_{w-in} - T_{w-out}) \quad (1)$$

where (\dot{V}_w) is the volume flow rate of the heat transfer fluid measured at the inlet. The heat exchange capacity rate (HXCR) indicates how fast heat is be transferred from the heat transfer fluid to the PCM. A high HXCR is desired for charging and discharging of the storage. The HXCR was expressed by the below equation [15]

$$HXCR = \dot{V}_w \rho_w C_{pw} \ln \left(\frac{T_{w-in} - T_{PCM}}{T_{w-out} - T_{PCM}} \right) \quad (2)$$

The stored or released energy of the PCM can be calculated by the below equation from the initial temperature to the final one [16]

$$Q_{PCM} = M [C_{ps} (T_s - T_{ini}) + C_{pa} (T_l - T_s) + C_{pl} (T_{fin} - T_l)] \quad (3)$$

where (M) is the mass of the phase change material. The supplied or extracted exergy of water can be calculated by the using the below equation [17]

$$EX_w = \dot{V}_w \rho_w C_{pw} \left[T_{w-in} - T_{w-out} - T_o \ln \frac{T_{w-in}}{T_{w-out}} \right] \quad (4)$$

where (T_o) is the dead state temperature of 25 °C. The total charged exergy is expressed as the sum of the exergy during solid state, two-phase state and liquid state, respectively [17].

$$EX_{PCM} = M C_{ps} \left[T_s - T_{ini} - T_o \ln \frac{T_s}{T_{ini}} \right] + M C_{pa} \left[T_l - T_s - T_o \ln \frac{T_l}{T_s} \right] \\ + M C_{pl} \left[T_{fin} - T_l - T_o \ln \frac{T_{fin}}{T_l} \right] \quad (5)$$

The exergy absorbed by the parabolic solar collector can be evaluated by [17]

$$EX_{coll} = A I \left[1 + \frac{1}{3} \left(\frac{T_o}{T_{sun}} \right)^4 - \frac{4}{3} \left(\frac{T_o}{T_{sun}} \right) \right] \quad (6)$$

where (A) is the collector area, (I) is the solar radiation and (T_{sun}) is the solar radiation temperature of 6000 K. The efficiency of the storage system is obtained based on the first law of thermodynamics and it is given by the ratio of the useful energy collected by the cold-water to the input energy by the solar radiation [12].

$$\eta_{en} = \frac{\text{Cold - water Heat Absorbed}}{\text{Solar Energy}} = \frac{\dot{V}_w \rho_w C_{pw} (T_{w-out} - T_{w-in})}{A I} \quad (7)$$

Like the storage energy efficiency of the system, the average storage exergy efficiency of system can be defined as the ratio of the useful exergy delivered by the cold water to the exergy absorbed by the solar collector [12].

$$\eta_{ex} = \frac{\text{Cold - water Exergy}}{\text{Collected Solar Exergy}} = \frac{EX_w}{EX_{coll}} \quad (8)$$

4. Results and Discussion

Energy and exergy analysis of the experimental transient behaviour of a multi PCMs system are discussed. The PCMs were investigated with three water flow rates of 0.5 L/min, 1 L/min, and 1.5 L/min. The water flow rate with its temperatures were measured alongside the temperature distribution of both capsules. During charging and discharging processes, liquid fraction, heat exchange capacity rate, energy, and exergy were calculated to be discussed with their efficiencies.

4.1 First Test (0.5 L/min Water Flow Rate)

The first test was performed on 25/8/2019. The average solar radiation was 517.6 W/m² while the maximum ambient temperature was 43.9 °C. The charging process lasts for 2.79 hours with an average hot-water temperature difference of 2.59 °C as shown in Figure 4. The first capsule with BHO took the heat directly from the hot water. The bottom temperature for both capsules increased faster than the top and middle temperatures due to the low water flow rate and high-water temperature. That showed a clear temperature distribution for both capsules after an amount of time. The first temperature started at 42.45 °C till 80°C while the second one started at 40.33 °C till 78.75 °C as shown in Figure 5. The first capsule started melting after 146 min and reached 99 % liquid at the end. The second capsule started melting after 75 min and liquidized completely at the minute of 129. The second capsule liquid fraction decreased from 50 % to 10.9 % in 15.7 min as its temperature drop due that the first capsule stored the most heat that coming from the water.

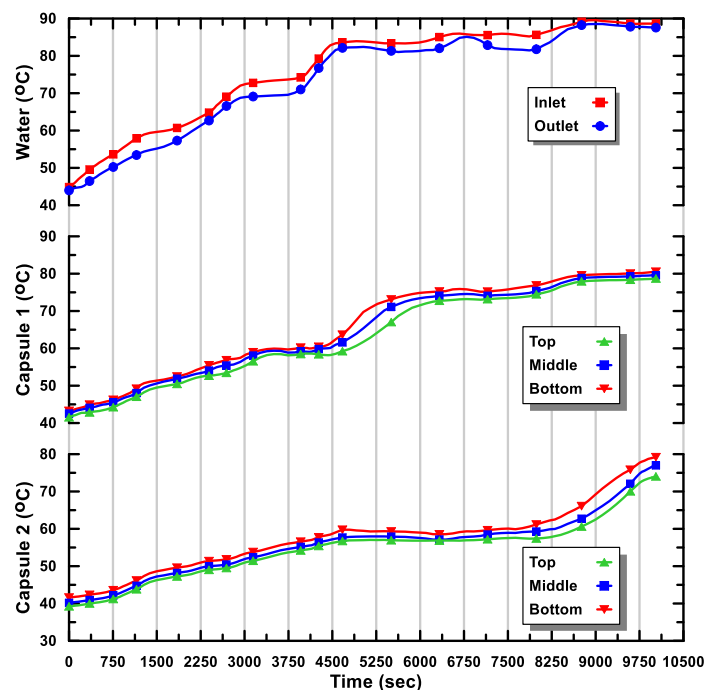


Fig. 4. Charging Process of the First Test

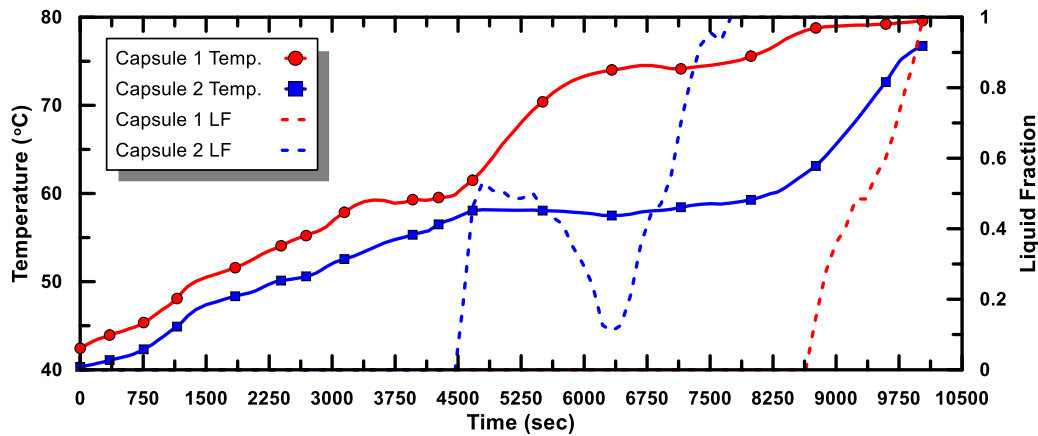


Fig. 5. Capsules Temperatures and Liquid Fractions During Charging

Figure 6 showed the heat transfer rate of the water, showing the variation of the water temperature difference with the water flow rate. At the starting of the two-phase for the second capsule, its HXCR matched that of the first capsule and stayed nearly constant to the end of the process due to the constant temperature of melting. The three regions of the second capsule – solid sensible heat, two-phase heat, and liquid sensible heat cannot be shown in the HXCR curve as it depends on the logarithmic temperature difference between the water and the PCM.

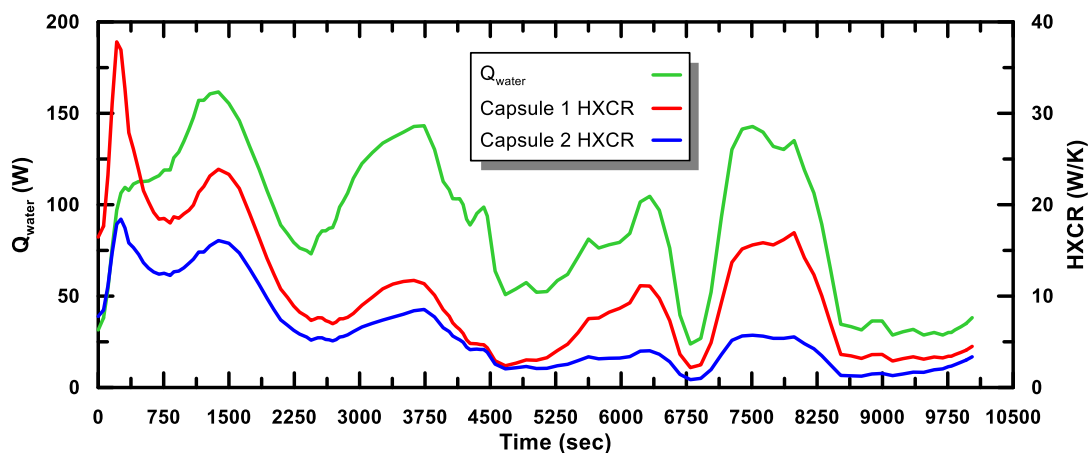


Fig. 6. Water Heat Transfer and PCM HXCR During Charging

The discharging process lasts for 2.27 hours after the finishing of the charging process with an average cold-water temperature difference of 5.84 °C and as shown in Figure 7. The first capsule had a two-phase and solid-phase solidification while the second capsule solidified from the liquid phase to the solid one bypassing the two-phase region. Figure 8 showed the average capsules temperature with their liquid fraction. The first capsule started at 79.96 °C in the two-phase region and solidified completely at 77.93 °C after 32 min to the end of the process at 45.85 °C. The second capsule started at 76.04 °C in the completely liquid region and reached a two-phase region at 61.28 °C after 28 min. Through more heat released, the PCM of the second capsule reached a point where it completely solidified at 59.83 °C for another 29 min to 41.72 °C at the end of the process. As the water temperature difference decreased in the middle of the process, the water heat transfer rate and the heat exchange capacity rate of both capsules decreased too as shown in Figure 9. There is a small difference between the HXCR of both capsules as their temperatures have a nearly constant trend after the second capsules solidified completely.

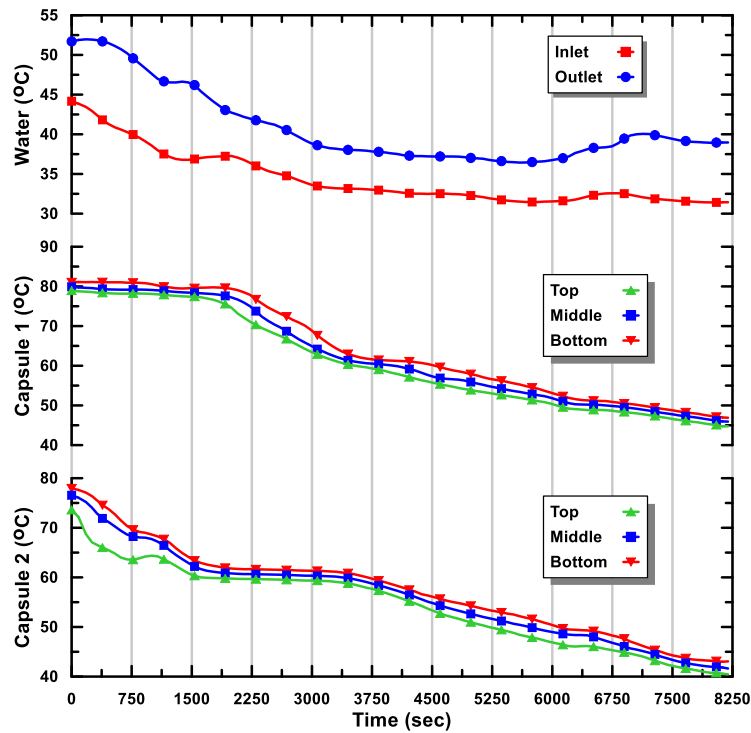


Fig. 7. Discharging Process of the First Test

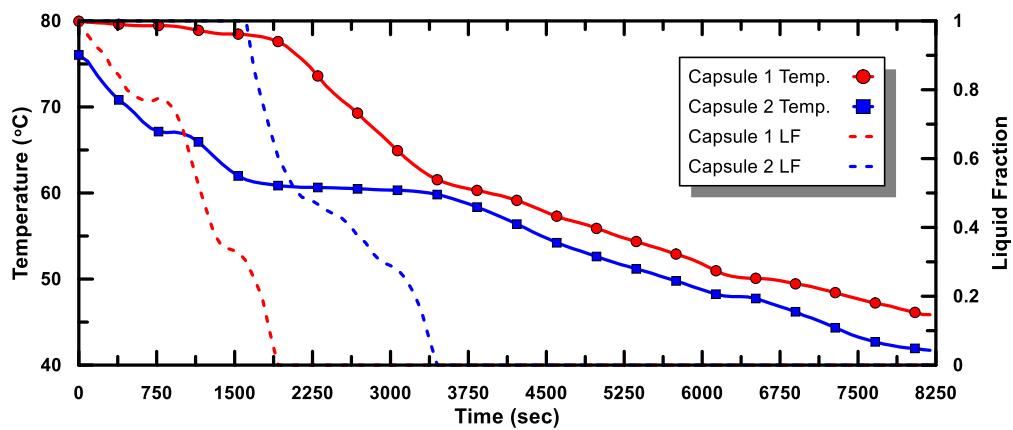


Fig. 8. Capsules Temperatures and Liquid Fractions During Discharging

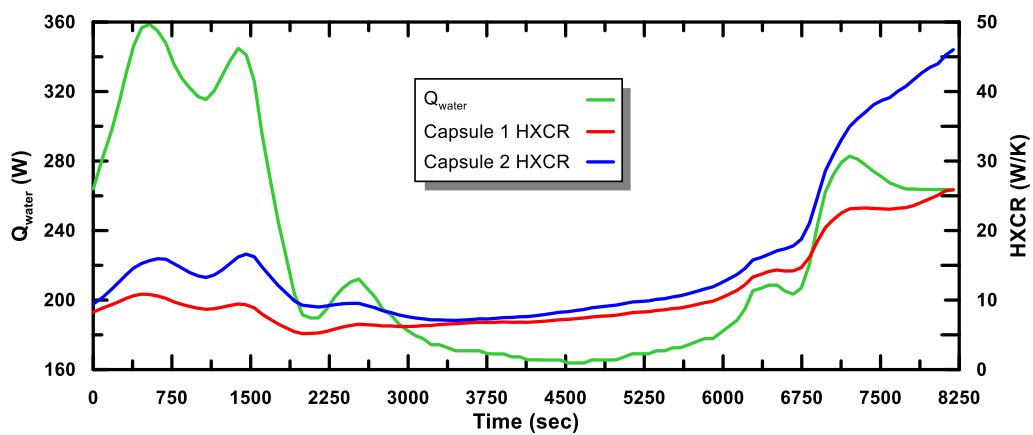


Fig. 9. Water Heat Transfer and PCM HXCR During Discharging

4.2 Second Test (1 L/min Water Flow Rate)

The second test was performed on 24/8/2019 with a 1 L/min water flow rate for both hot and cold sides. The average solar radiation was 495.2 W/m^2 while the maximum ambient temperature was $42.1 \text{ }^\circ\text{C}$. The charging process lasted for 4.84 hours with an average hot-water temperature difference of $1.44 \text{ }^\circ\text{C}$ as shown in Figure 10. The temperature distribution of the first capsule has a clear temperature difference due to the different melting points and heat capacities of the second capsule. The first capsule stored energy in the solid sensible and the two-phase regions. The second capsule stored energy in the sensible regions of both solid and liquid as well as in the two-phase regions. Figure 11 showed the average capsules temperature with their liquid fraction. The first temperature started at $37.41 \text{ }^\circ\text{C}$ to $82.61 \text{ }^\circ\text{C}$ while the second one started at $35.58 \text{ }^\circ\text{C}$ to $79.2 \text{ }^\circ\text{C}$. The two-phase process of the first capsule lasts for 69.8 minutes that started after 221 minutes of charging to 99.5 % of liquid fraction. The two-phase region lasted for about 96 min while the liquid region lasted for 93 min. The liquid fraction of the second capsule started after 101.8 min from the beginning of the charging. Due to the different melting point of both PCMs and the variation of the temperature distribution of the first capsule, the temperature of the second capsule dropped in different locations during the two-phase transition, that led to small solidifications during that process. Figure 12 showed the water heat transfer and the heat exchange capacity rate of the PCM. The average heat transfer of water was 101.12 W . The capacity rate of the first capsule was higher than that of the second one due to the high melting temperature and its enclosure is attached to the water flowing enclosure. The first and second HXCR was nearly constant during the phase change of the second capsule with average values of 6.86 W/K and 3.43 W/K for both first and second capsules respectively. The values were increased to 25.86 W/K and 13.84 W/K respectively, at the end of the process as the water temperature difference increased to $1.46 \text{ }^\circ\text{C}$ due to more heat-absorbing of the liquid region of the second capsule.

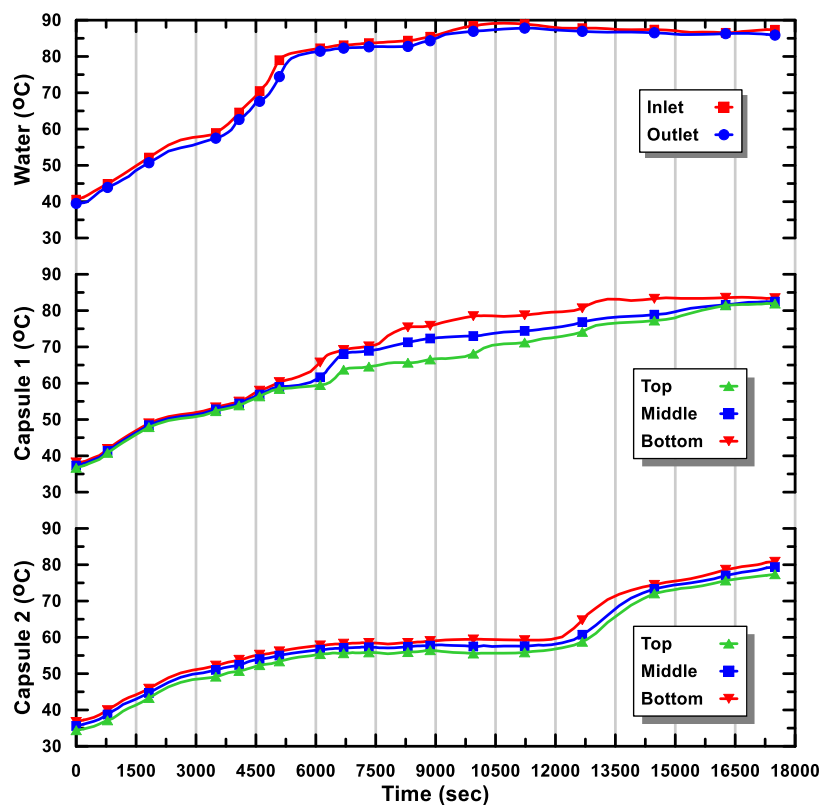


Fig. 10. Charging Process of the Second Test

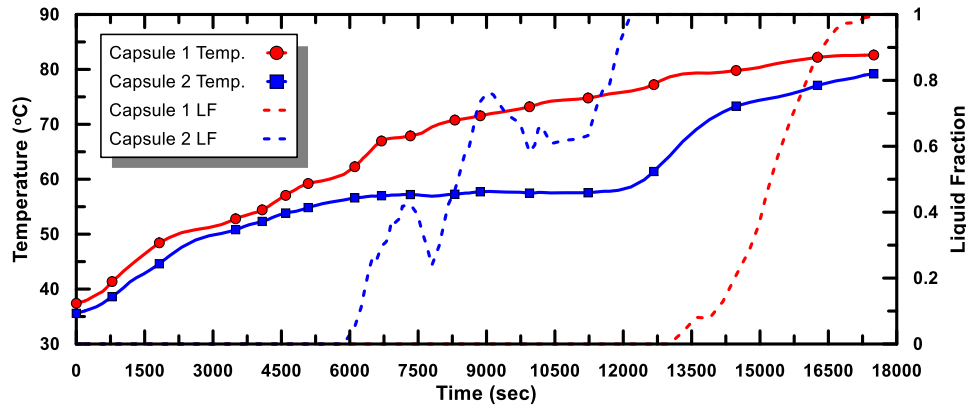


Fig. 11. Capsules Temperatures and Liquid Fractions During Charging

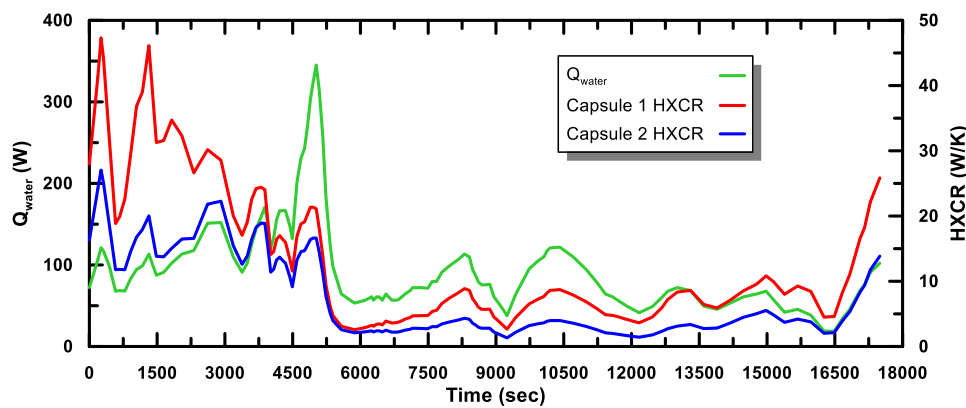


Fig. 12. Water Heat Transfer and PCM HXCR During Charging

The discharging process lasts for 2.51 hours with an average cold-water temperature difference of 3.92 °C as shown in Figure 13. The first capsule temperatures decreased through time and maintain nearly the same temperature distribution after 86 min of discharging. The second capsule temperature distribution disarranged at the sensible heat transfer at the beginning and the ending but maintains a constant difference during the phase transition. Figure 14 showed the average capsules temperature with their liquid fraction. The first and second capsule initial temperatures were 79.39 °C and 73.68 °C respectively and the final temperatures were at 44.19 °C and 36.9 °C respectively. The first capsule began with the two-phase solidification that lasted about 26.3 minutes to 77.85 °C where it got completely solid. The second capsule began with the sensible liquid region that lasted about 27.8 minutes to 59.69 °C where it began to solidify. Then the two-phase region started with the last temperature and finished at 57.4 °C where it completely solidified. That process took about 42.8 minutes to done and continued with the temperature decreasing through the sensible solid region. Due to low storing energy at the sensible solid region, the water temperature difference got decreased and that led to lowering the water heat rate as shown in Figure 15. The average HXCR for the first and second capsules were 13.93 W/K and 24.27 W/K respectively.

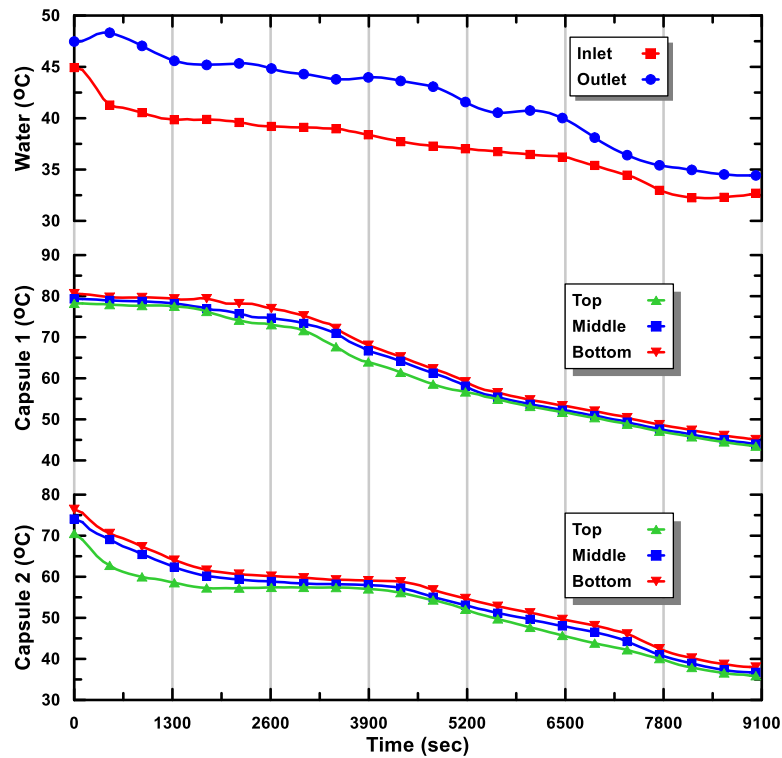


Fig. 13. Discharging Process of the Second Test

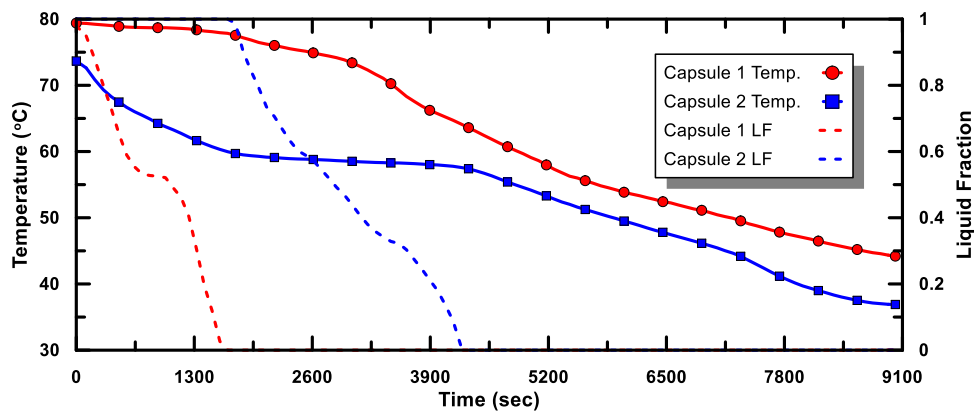


Fig. 14. Capsules Temperatures and Liquid Fractions During Discharging

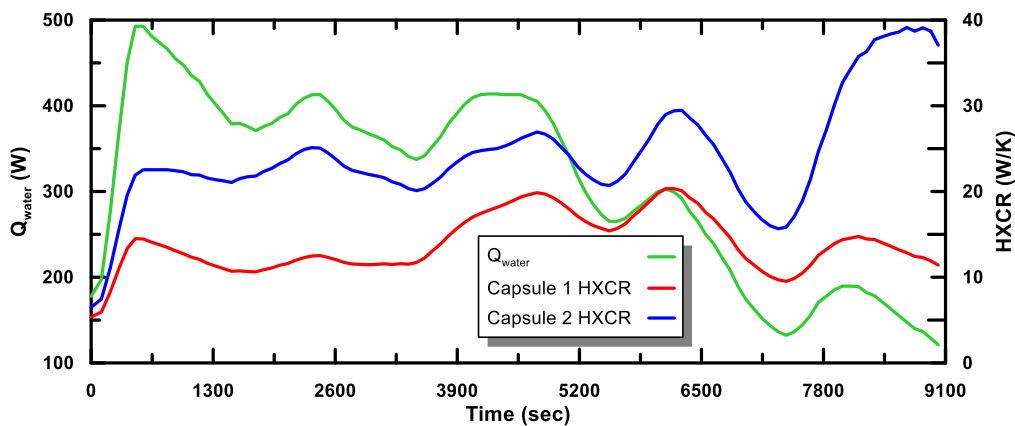


Fig. 15. Water Heat Transfer and PCM HXCR During Discharging

4.3 Third Test (1.5 L/min Water Flow Rate)

The third test was performed on 29/8/2019 with a 1.5 L/min water flow rate for hot and cold sides. The average solar radiation was 481.8 W/m^2 while the maximum ambient temperature was $41.7 \text{ }^\circ\text{C}$. The charging process lasts for 5.19 hours with an average hot-water temperature difference of $1.12 \text{ }^\circ\text{C}$ as shown in Figure 16. The temperature distribution of the first capsule increased with the same rate through time with the bottom temperature higher than the middle and top temperatures. After 3 hours the bottom temperature of the second capsule increases faster than the above two.

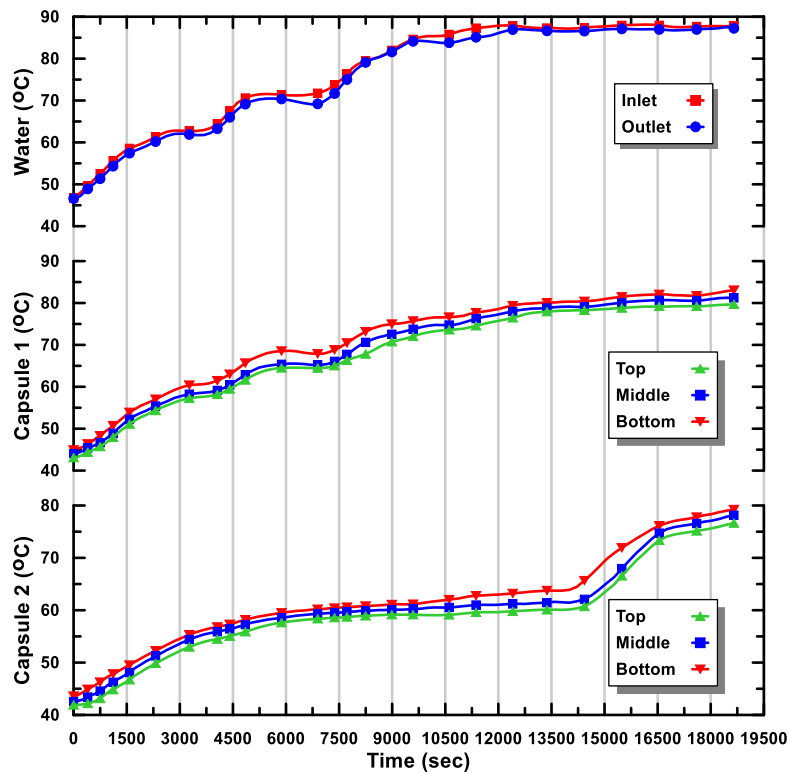


Fig. 16. Charging Process of the Third Test

Figure 17 showed the average capsules temperature with their liquid fraction. As the BHO has a higher melting point than the SAT, the latent heat time of the BHO is lower than that of the SAT while the solid sensible time of the BHO was more than that of the SAT. The first capsule started at $44.03 \text{ }^\circ\text{C}$ till $81.34 \text{ }^\circ\text{C}$ while the second capsule started at $42.7 \text{ }^\circ\text{C}$ till $78 \text{ }^\circ\text{C}$. The two-phase region of the first capsule started with $78.52 \text{ }^\circ\text{C}$ to the final temperature through 98.6 min. The two-phase region of the second capsule started with $58.75 \text{ }^\circ\text{C}$ to $61.82 \text{ }^\circ\text{C}$ where it got completely liquified through 128 min. The average water heat transfer rate was 117.2 W where it decreased to 5.23 W after 2.3 hours from the beginning as shown in Figure 18 due to the low water temperature difference caused by a low flow rate. The average HXCR of the first capsule is higher than that of the second with 19.48 W/K and 9.65 W/K respectively.

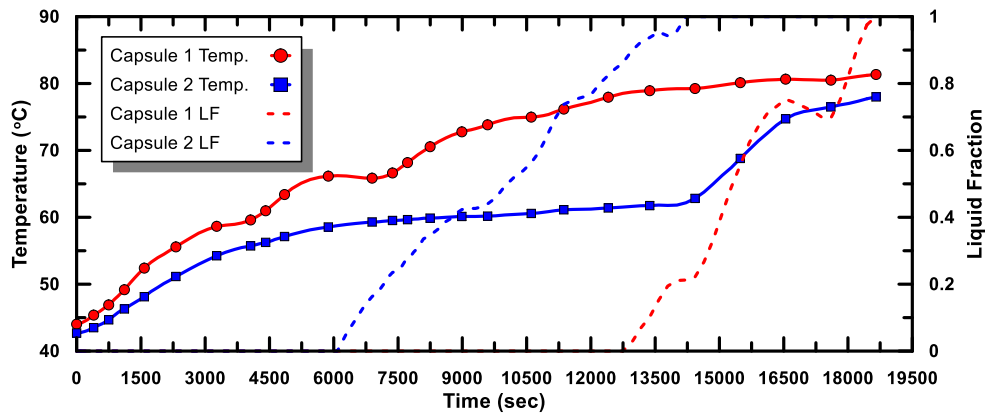


Fig. 17. Capsules Temperatures and Liquid Fractions During Charging

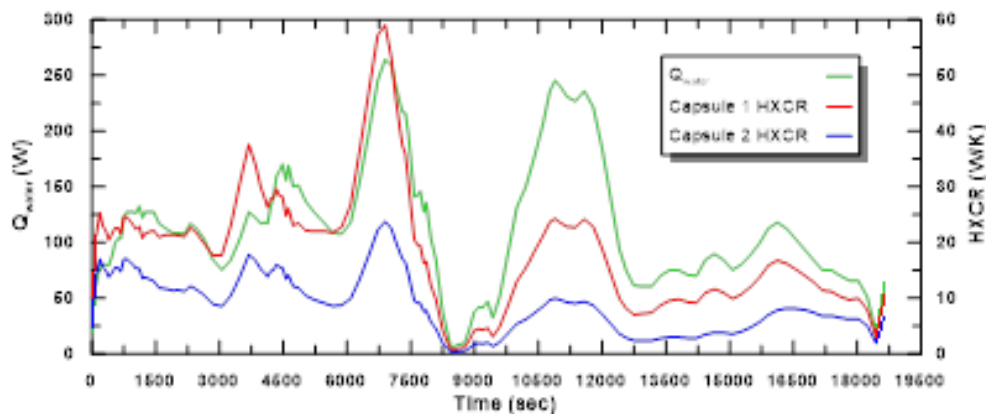


Fig. 18. Water Heat Transfer and PCM HXCR During Charging

The discharging process lasts for 3.73 hours with an average cold-water temperature difference of 2.91 °C as shown in Figure 19. For a quarter an hour, the cold temperature difference of water was less than 1 °C. The first capsule temperature distribution decreased through time as well as the second one. The second capsule temperature distribution decreased with time with a small difference between the top, middle, and bottom temperatures. With a 1.5 L/min water flow rate, the whole salt inside the second capsule rejected the heat simultaneously. Figure 20 showed the average capsules temperature with their liquid fraction. The first capsule started at 81.33 °C to the end of the solidification process at 41.44 °C while the second capsule started at 78.14 °C to 38.79 °C at the end of the same process. The two-phase region period of the first capsule was 64.8 minutes while that of the second capsule was 52.7 minutes. Both capsules liquid fractions followed the same slop of decreasing as they have 12.1 minutes in their two-phase period. As the temperature of PCM is closer to the water temperature, its HXCR became higher. During the discharging process, the HXCR of the second capsule was higher than that of the first. Figure 21 showed the temperature difference of water decreased after 4500 seconds as the first and second capsules finished their two-phase heat transition. So, the heat transfer rate of water decreased.

From Figure 22, It is clear that the second capsule of the SAT reached the liquid phase for all the tests. The first capsule of BHO reached the two-phase region and cannot be extended to the liquid phase due to the long charging period. Also, the higher the water flow rate, the longer the charging and discharging times.

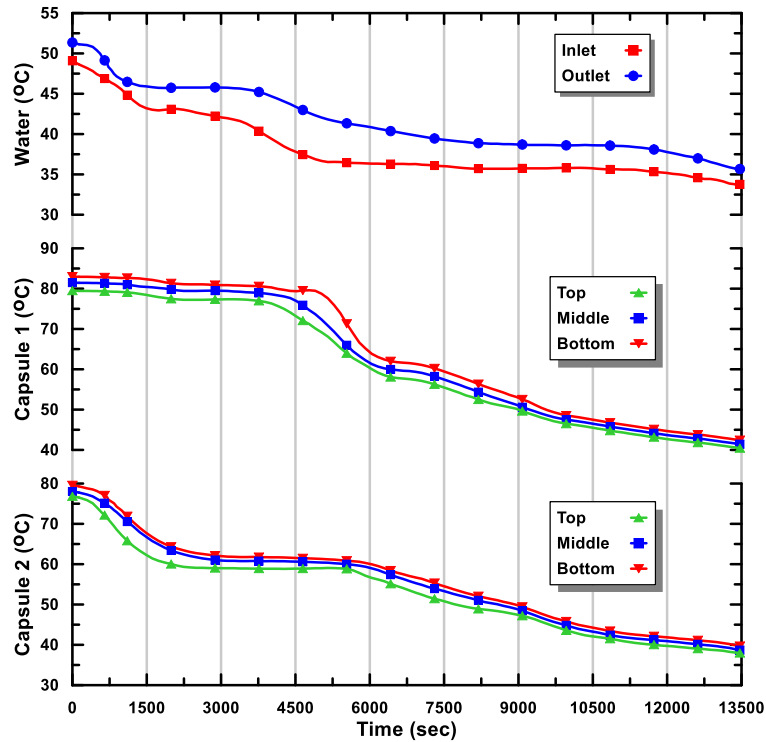


Fig. 19. Discharging Process of the Third Test

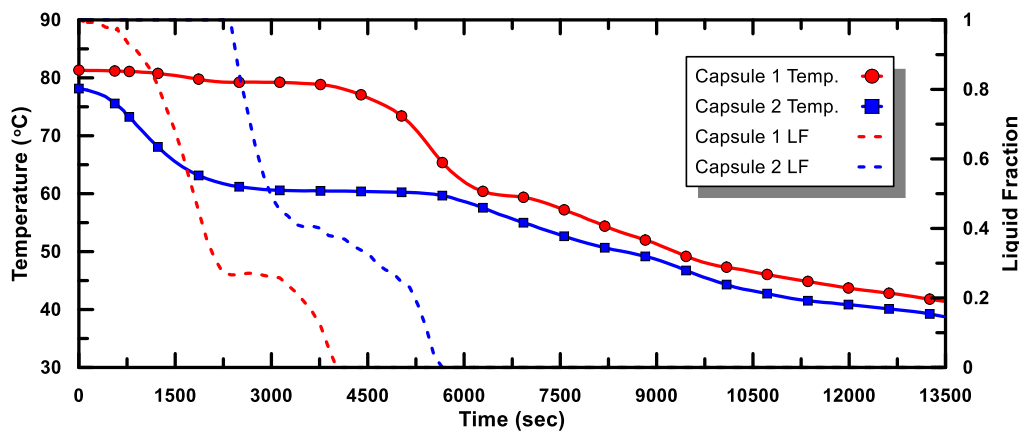


Fig. 20. Capsules Temperatures and Liquid Fractions During Discharging

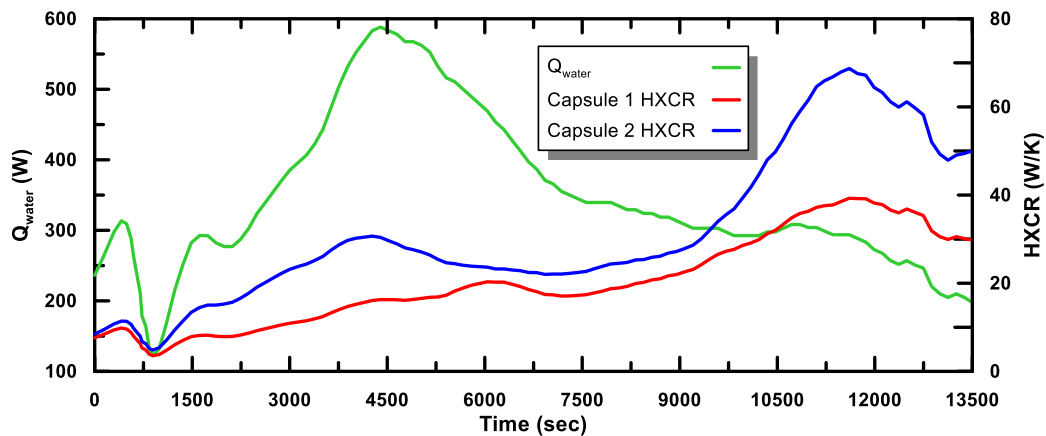


Fig. 21. Water Heat Transfer and PCM HXCR During Discharging

4.4 Tests Comparison

The sequence of the charging process and how the liquid fraction can be seen from the glasses cover of both capsules at the starting of the charging, the middle of the two-phase transition, and at the end of the charging process are shown in Table 2. The first capsule is on the right while the second one is on the left. As it is hard to tell the exact liquidous temperature without entering the liquid sensible state, the final temperature of the charging process for the BHO was assumed as the liquidous temperature of the PCM. The red lines represented the solid area.

Table 2
 Melting Profile of the Second Case

Water Flow Rate	Starting Time	Middle of the Two-Phase Time	Ending Time
0.5 LPM			
1 LPM			
1.5 LPM			

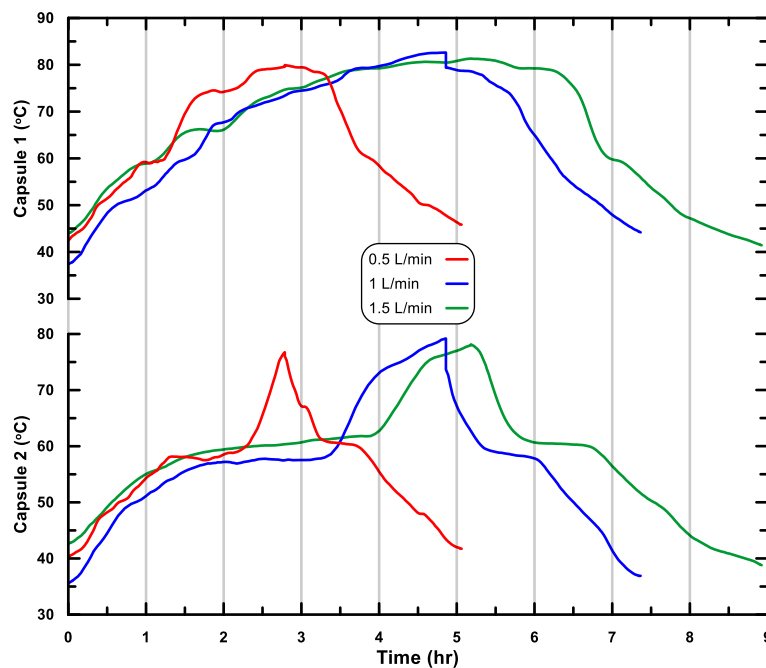


Fig. 22. Capsules Temperatures During Charging and Discharging

The energy of the charging and discharging processes are the summation of the sensible heat of the solid-phase, the latent heat of the two-phase, and the sensible heat of the liquid-phase if exists. Figure 23 shows that the energy of the charging process is higher than that of the discharging process for both capsules and for all the tests except the last one as it may refer to some human errors. From the figure, it can be seen that the 0.5 L/min and 1.5 L/min tests have nearly the same energy storage and released for the first capsule. The 1 L/min test has the highest energy storage for both capsules. For the second capsule, as all the test have two sensible heat transfers alongside with the latent heat, its charging and discharging energies were higher than that of the first capsule. The charging and discharging exergy of the first and second capsules for all the tests are shown in Figure 24. As the BHO has higher melting enthalpy than the SAT, its storing exergy was the highest. The highest storing exergy for the first capsule was due to 1 L/min while for the second capsule due to 1.5 L/min. Even that, these tests did not specify the best water flow rate for the highest storing energies and exergies, as they all have small differences among them. The true measure about the best test can be told the efficiencies of the system, based on the energy and exergy analysis. As shown in Figure 25, the energy and exergy efficiencies increased with increasing the water flow rate. The 1.5 L/min has the highest energy and exergy efficiencies even that it has 6.34 % and 1.21 % differences with the 1 L/min test for the energy and exergy efficiencies respectively.

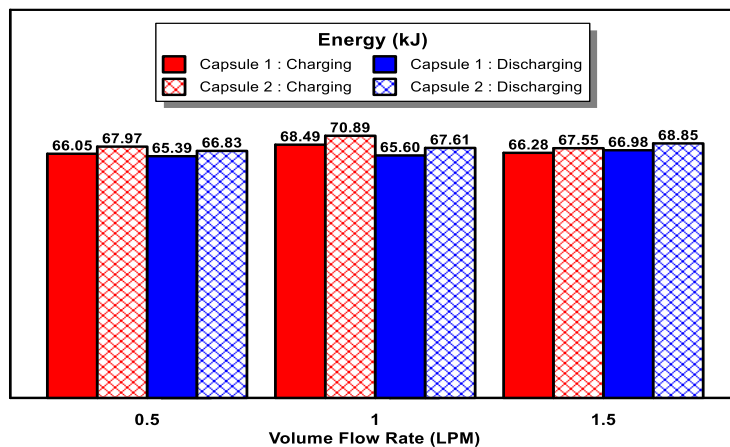


Fig. 23. The Energy of the Charging and Discharging

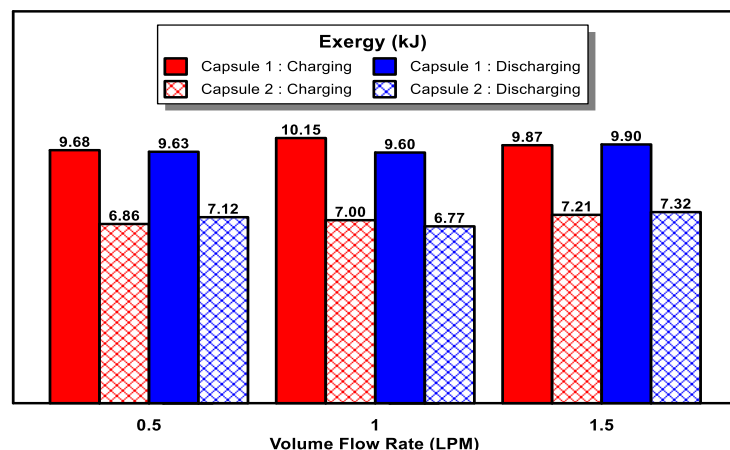


Fig. 24. The Exergy of the Charging and Discharging

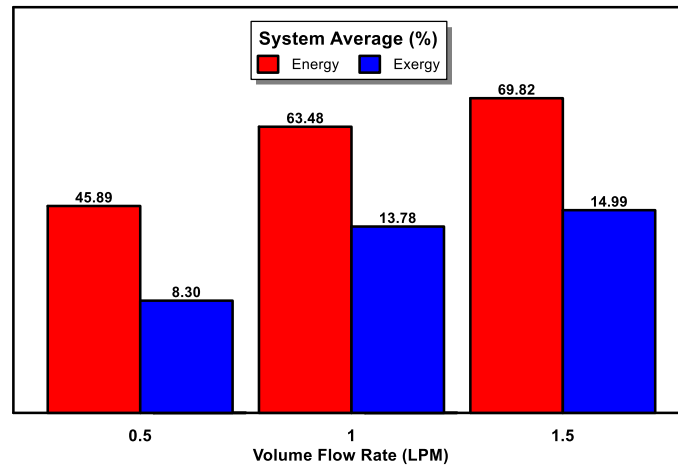


Fig. 25. Average Energy and Exergy Efficiencies

4. Conclusion

The following conclusion can be derived from the experimental results on the performance of a multi PCM system. With the Barium Hydroxide Octahydrate inside the first capsule and the Sodium Acetate Trihydrate inside the second capsule, some remarks can be summarized as below

- i. In general, the increase in the water flow rate increases the time required to melt the PCM and decreases the temperature difference of the charging water.
- ii. The charging time is longer than the discharging time as the hot water temperature difference during melting was lower than that of the solidification.
- iii. For the 0.5 L/min water flow rate, the charging period is 2.79 hours with an average hot-water temperature difference of 2.59 °C, while the discharging period is 2.27 hours with an average cold-water temperature difference of 5.84 °C.
- iv. For the 1 L/min water flow rate, the charging period is 4.84 hours with an average hot-water temperature difference of 1.44 °C, while the discharging period is 2.51 hours with an average cold-water temperature difference of 3.92 °C.
- v. For the 1.5 L/min water flow rate, the charging period is 5.19 hours with an average hot-water temperature difference of 1.12 °C, while the discharging period is 3.73 hours with an average cold-water temperature difference of 2.91 °C.
- vi. The 1 L/min water flow rate gives a maximum total storage energy of 139.38 kJ and maximum total storage exergy of 17.15 kJ.
- vii. The 1.5 L/min water flow rate gives maximum system energy efficiency of 64.82 % and maximum system exergy efficiency of 14.99 %.

References

- [1] Garshasbi, Samira, and Mat Santamouris. "Using advanced thermochromic technologies in the built environment: Recent development and potential to decrease the energy consumption and fight urban overheating." *Solar Energy Materials and Solar Cells* 191 (2019): 21-32. <https://doi.org/10.1016/j.solmat.2018.10.023>
- [2] Zeyghami, Mehdi, D. Yogi Goswami, and Elias Stefanakos. "A review of clear sky radiative cooling developments and applications in renewable power systems and passive building cooling." *Solar Energy Materials and Solar Cells* 178 (2018): 115-128. <https://doi.org/10.1016/j.solmat.2018.01.015>
- [3] Pielichowska, Kinga, and Krzysztof Pielichowski. "Phase change materials for thermal energy storage." *Progress in materials science* 65 (2014): 67-123. <https://doi.org/10.1016/j.pmatsci.2014.03.005>
- [4] Sarbu, I., and C. Sebarchievici. "Chapter 7-Solar Thermal-Driven Cooling Systems." *Solar Heating and Cooling Systems* (2017): 241-313. <https://doi.org/10.1016/B978-0-12-811662-3.00007-4>

- [5] Salunkhe, Pramod & Devanuri, Jaya Krishna. (2017). Investigations on latent heat storage materials for solar water and space heating applications. *Journal of Energy Storage*. 12. 243-260. <https://doi.org/10.1016/j.est.2017.05.008>
- [6] Englmaier, Gerald, Christoph Moser, Hermann Schranzhofer, Jianhua Fan, and Simon Furbo. "A solar combi-system utilizing stable supercooling of sodium acetate trihydrate for heat storage: Numerical performance investigation." *Applied Energy* 242 (2019): 1108-1120. <https://doi.org/10.1016/j.applthermaleng.2019.114647>
- [7] Wang, Qian, Jiangtao Wang, Yunyu Chen, and C. Y. Zhao. "Experimental investigation of barium hydroxide octahydrate as latent heat storage materials." *Solar Energy* 177 (2019): 99-107. <https://doi.org/10.1016/j.solener.2018.11.013>
- [8] Elfeky, K. E., N. Ahmed, and Qiuwang Wang. "Numerical comparison between single PCM and multi-stage PCM based high temperature thermal energy storage for CSP tower plants." *Applied Thermal Engineering* 139 (2018): 609-622. <https://doi.org/10.1016/j.applthermaleng.2018.04.122>
- [9] Thomson, A., and Gianfranco Claudio. "The Technical and Economic Feasibility of Utilising Phase Change Materials for Thermal Storage in District Heating Networks." *Energy Procedia* 159 (2019): 442-447. <https://doi.org/10.1016/j.egypro.2018.12.042>
- [10] Suffer, Kadhim Hussein, Jalal M. Jalil, and Hiba A. Hasan. "Numerical Investigation of PCM Thermal Storage in Water Solar Collector." *Journal of Advanced Research in Fluid Mechanics and Thermal Sciences* 66 (2020): 164-178. <https://doi.org/10.1016/j.ast.2012.02.006>
- [11] Bayomy, Ayman, Stephen Davies, and Ziad Saghir. "Domestic Hot Water Storage Tank Utilizing Phase Change Materials (PCMs): Numerical Approach." *Energies* 12, no. 11 (2019): 2170. <https://doi.org/10.3390/en12112170>
- [12] Nagappan, Beemkumar, Karthikeyan Alagu, Yuvarajan Devarajan, and Dinesh Babu Munuswamy. "Energy and exergy analysis of multi-temperature PCMs employed in a latent heat storage system and parabolic trough collector." *Journal of Non-Equilibrium Thermodynamics* 43, no. 3 (2018): 211-220. <https://doi.org/10.1515/jnet-2017-0066>
- [13] Li, Bin, Xiaoqiang Zhai, and Xiwen Cheng. "Experimental and numerical investigation of a solar collector/storage system with composite phase change materials." *Solar Energy* 164 (2018): 65-76. <https://doi.org/10.1016/j.solener.2018.02.031>
- [14] Hosseininiasab, Seyedalireza, and Ebrahim Nematy Lay. "Critical Modeling & Exergy Analysis of Multi Phase Change Materials Storage System." *Chemical Product and Process Modeling* 13, no. 1 (2017). <https://doi.org/10.1515/cppm-2017-0029>
- [15] Dannemand, Mark, Weiqiang Kong, Jakob B. Johansen, and Simon Furbo. "Laboratory test of a cylindrical heat storage module with water and sodium acetate trihydrate." *Energy Procedia* 91 (2016): 122-127. <https://doi.org/10.1016/j.egypro.2016.06.186>
- [16] Huang, Huajie, Zilong Wang, Hua Zhang, Binlin Dou, Xiuhui Huang, Hao Liang, and Maria A. Goula. "An experimental investigation on thermal stratification characteristics with PCMs in solar water tank." *Solar Energy* 177 (2019): 8-21. <https://doi.org/10.1016/j.solener.2018.11.004>
- [17] Yang, Lei, Xiaosong Zhang, and Guoying Xu. "Thermal performance of a solar storage packed bed using spherical capsules filled with PCM having different melting points." *Energy and buildings* 68 (2014): 639-646. <https://doi.org/10.1016/j.enbuild.2013.09.045>